

# Electron acceleration from contracting magnetic islands during reconnection

J. F. Drake<sup>1</sup>, M. Swisdak<sup>2</sup>, H. Che<sup>1</sup> & M. A. Shay<sup>3</sup>

A long-standing problem in the study of space and astrophysical plasmas is to explain the production of energetic electrons as magnetic fields ‘reconnect’ and release energy. In the Earth’s magnetosphere, electron energies reach hundreds of thousands of electron volts (refs 1–3), whereas the typical electron energies associated with large-scale reconnection-driven flows are just a few electron volts. Recent observations further suggest that these energetic particles are produced in the region where the magnetic field reconnects<sup>4</sup>. In solar flares, upwards of 50 per cent of the energy released can appear as energetic electrons<sup>5,6</sup>. Here we show that electrons gain kinetic energy by reflecting from the ends of the contracting ‘magnetic islands’ that form as reconnection proceeds. The mechanism is analogous to the increase of energy of a ball reflecting between two converging walls—the ball gains energy with each bounce. The repetitive interaction of electrons with many islands allows large numbers to be efficiently accelerated to high energy. The back pressure of the energetic electrons throttles reconnection so that the electron energy gain is a large fraction of the released magnetic energy. The resultant energy spectra of electrons take the form of power laws with spectral indices that match the magnetospheric observations.

The narrow current layers that form at the X-line during particle-in-cell simulations of magnetic reconnection spawn secondary magnetic islands<sup>7</sup> (Fig. 1a, b), suggesting that the interaction of multiple magnetic islands is intrinsic to the dynamics of reconnection and associated particle acceleration. Electron acceleration during reconnection and island formation is reflected in the strong increase in the electron temperature parallel to the local magnetic field,  $T_{e\parallel}$ , in the simulation data (Fig. 1c). While some of these energetic electrons are produced as a result of acceleration by parallel electric fields near the magnetic separatrices and subsequent injection into the islands, electrons within the islands continue to gain energy. The energy gain, however, is not the result of a parallel electric field, which is very small within magnetic islands<sup>8,9</sup>. The outflows from the magnetic X-lines cause the ends of the islands to move inward at the Alfvén speed. Particles circulating within the magnetic islands gain energy in a classic Fermi manner as they reflect from the moving ends of the islands (Fig. 2a, b). At the same time, the particles slowly drift outwards until they cross the separatrix and leave the island. The energy in the parallel motion is scattered into the perpendicular motion during the separatrix crossing (Fig. 2c)<sup>10</sup>. A similar Fermi process has been studied during Earthward-directed flows in the near-Earth region of the magnetotail<sup>11</sup>, and is evident in the data of test particles in multi-island magnetohydrodynamic models<sup>12,13</sup>.

The rate of gain of the parallel energy  $\varepsilon_{\parallel}$  during reflection from the ends of magnetic islands contracting with a velocity  $u_x$  can be

calculated analytically (Fig. 2),

$$\frac{d\varepsilon_{\parallel}}{dt} = -2\varepsilon_{\parallel} \frac{u_x B_x^2}{\delta_x B^2} \quad (1)$$

where  $2\delta_x$  is the length of the island, and  $B_x$  and  $B$  are the reconnecting and total magnetic fields. Equation (1) is independent of mass so that the rate of energy gain is the same for electrons and ions. However, the equation is only valid for particles with large parallel velocity  $v_{\parallel} \gg u_x \approx c_{Ax}$ , with  $c_{Ax}$  the Alfvén speed, so only the motion of very energetic ions is described by equation (1). Equation (1) can be integrated to obtain the invariant action ( $\varepsilon_{\parallel}^{1/2} \delta_x$  for small  $B_x$ ). Thus, the energy gain of the particles in a given island is limited by the change in the island geometry. To reach very high energies, particles must therefore interact with many islands. The trajectory of the particle in Fig. 2 suggests that this is a likely scenario.

The efficiency of electron heating by the Fermi mechanism is confirmed in particle simulations of the contraction of squashed flux bubbles (Fig. 3). An important question is how the back pressure from energetic particles limits island contraction. Using equation (1), the increase in the particle energy can be combined with the released magnetic energy to obtain an expression for the total energy change  $dW$  during an increment in the island length  $d\delta_x$ :

$$dW = 2 \frac{d\delta_x}{\delta_x} \frac{B_x^2}{8\pi} \left( 1 - \frac{8\pi \bar{\varepsilon}_{\parallel}}{B^2} \right) \quad (2)$$

where the bar over  $\varepsilon_{\parallel}$  denotes an average over the distribution of particle velocities. For negative  $d\delta_x$ , magnetic energy is released while electrons increase their energy and therefore inhibit contraction. When the back pressure of the energetic particles approaches the local magnetic energy density, island contraction ceases and halts the transfer of energy from the magnetic field into the energetic particles (Fig. 3c). Fermi acceleration during island contraction is therefore self-limiting and links the energy gain of particles to the released magnetic energy.

In a three-dimensional system, unless the ambient guide field is close to zero, magnetic islands are not constrained to form a single chain along the symmetry line of a current layer but can form at other locations<sup>14</sup>. Islands therefore should be volume filling in a region around a large-scale X-line (Fig. 4a). In such a picture, islands form, grow and contract. After contraction, the magnetic energy having been released, the island merges with a neighbour (lower current layer in Fig. 1b), completing its life cycle. Particles gain energy through Fermi acceleration in a sequence of islands. The shocks associated with many small islands may also accelerate particles<sup>15</sup>. As it is not possible to simulate a large-scale system in a three-dimensional kinetic model, we develop a transport model of particle heating. We average the energy gain equation over many islands (Fig. 4a), taking into account the scattering of energy from the parallel to the

<sup>1</sup>University of Maryland, College Park, Maryland 20742, USA. <sup>2</sup>Plasma Physics Division, Naval Research Laboratory, Washington DC 20375, USA. <sup>3</sup>University of Delaware, Newark, Delaware 19716, USA.

perpendicular direction, and construct an equation for the omnidirectional distribution function  $F(x, y, v) \equiv v^2 f(x, y, v)$ :

$$\nabla \cdot \mathbf{u}F - \nabla \cdot \mathbf{D} \cdot \nabla F = -\frac{A}{3} \left( 1 - \frac{8\pi\bar{\varepsilon}}{3B^2} \right)^{\frac{1}{2}} \frac{dC_{Ax}}{dy} \frac{\partial}{\partial v} vF \quad (3)$$

where  $f(x, y, v)$  is the particle phase space density,  $\mathbf{u}$  is the local plasma velocity,  $\mathbf{D}$  is the diffusion rate<sup>16</sup> and  $\bar{\varepsilon} = 3\varepsilon_{\parallel}$ . This equation describes the balance between the Fermi drive and the energy loss associated with convection and diffusion, including the back pressure from energetic particles. It is similar to that describing particle acceleration in shocks<sup>17</sup>. We solve this equation in the flow geometry shown in Fig. 4a, where the half-widths of the region of contracting islands are given by  $\Delta_y$  and  $\Delta_x$  in the inflow and outflow directions, respectively. Within the region of overlapping islands, convection is the dominant loss mechanism and the energy spectrum can be calculated analytically (see Supplementary Information):

$$F(v) = \frac{2\sigma - 1}{v^{2\sigma}} \int_0^v dq q^{2\sigma-1} F_{\text{in}}, \quad \sigma = \frac{1}{2} \left( \frac{1}{\hat{A}} + 1 \right) \quad (4)$$

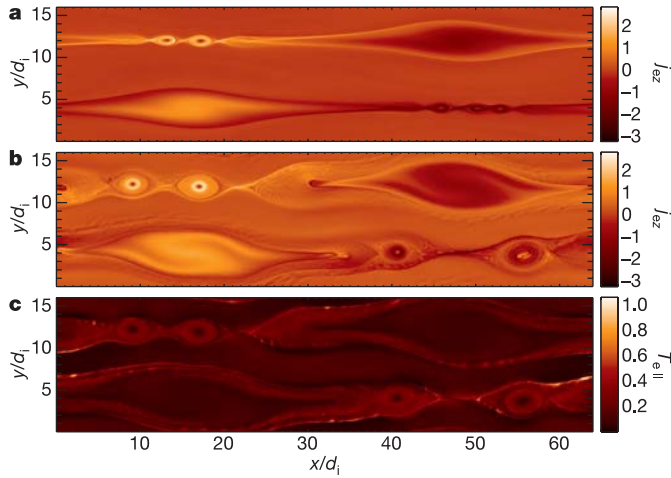


**Figure 1 | Computer simulations of island formation and electron acceleration during magnetic reconnection.** Particle-in-cell simulations using the p3d code<sup>22</sup> are performed in doubly periodic two-dimensional geometry starting with two Harris current sheets with a peak density of  $n_0$  superimposed on an ambient population of uniform density ( $0.2n_0$ ). The reconnection magnetic field is:

$$B_x/B_0 = \tanh[(y - L_y/4)/w_0] - \tanh[(y - 3L_y/4)/w_0] - 1$$

where  $B_0$  is the asymptotic magnetic field,  $w_0 = 0.5d_i$ ,  $L_x = 64d_i$  and  $L_y = 16d_i$  are the half-width of the initial current sheets and the box size in the  $x$  and  $y$  directions. The electron and ion temperatures, respectively  $T_e/m_e c_A^2 = 1/12$  and  $T_i/m_i c_A^2 = 5/12$ , are initially uniform as is the initial out-of-plane ‘guide’ field  $B_z/B_0 = 1.0$ . The ion inertial length is given by  $d_i = c/\omega_{pi}$  with  $\omega_{pi} = (4\pi n_0 e^2/m_i)^{1/2}$  and the Alfvén speed is given by  $c_A = B_0/(4\pi m_i n_0)^{1/2}$ . The electron mass  $m_e$  is taken to be  $0.01m_i$  and the velocity of light  $c = 20c_A$ . The spatial grid consists of  $4,096 \times 1,024$  cells with 100 particles per cell in the ambient background. The electron out-of-plane current  $j_{ez}$  is shown at two times:  $t = 14.0\Omega_{ci}^{-1}$  in **a** and  $t = 20.0\Omega_{ci}^{-1}$  in **b**, where  $\Omega_{ci} = eB_0/m_i c$  is the ion cyclotron frequency. The spontaneous formation and growth of secondary magnetic islands is evident. The repeated breakup of X-line current layers is typical of guide-field reconnection where narrow current layers promote secondary island formation<sup>7</sup>. The electron temperature parallel to the local magnetic field,  $T_{e\parallel}$ , is shown at  $t = 20.0\Omega_{ci}^{-1}$  in **c**. Seen is intense heating around the rims of the islands, which results from the acceleration of the electrons by parallel electric fields near the magnetic separatrices<sup>8,9</sup>, and heating within the magnetic islands. The localization of the parallel electric field to the vicinity of the separatrix reduces its importance as an electron accelerator. The Fermi mechanism dominates when  $v_{\parallel}$  exceeds the electron Alfvén speed  $c_{Aex} = B_x/\sqrt{4\pi n m_e}$ , which corresponds to an energy of 10 keV in the Earth’s magnetotail.

where  $\hat{A} = A\Delta_x/(3\Delta_y)$  is the normalized Fermi drive,  $F_{\text{in}}$  is the upstream value of  $F$  and we have ignored the back pressure from the energetic particles. The distribution function at high energy takes the form of a power law with an index that depends on the mean aspect ratio of the individual magnetic islands and the island region through  $\hat{A}$ . Numerical solutions to equation (3) for  $F$  confirm the power-law behaviour (Fig. 4b, c). The aspect ratio of the magnetic islands, and therefore  $\hat{A}$  and  $\sigma$ , remain uncertain. For  $\hat{A} > 0.5$  or  $\sigma < 1.5$ , the energy integral of the energetic particles  $\bar{\varepsilon}$  diverges unless the back pressure of energetic particles is included. Retaining the back pressure, the energy content of electrons rises until  $\bar{\varepsilon} \approx B^2/8\pi$ . The back pressure throttles the Fermi drive and the spectral index of the energetic particles can be characterized by the upstream value of the electron thermal ( $p_{e0}$ ) to magnetic pressure ratio  $\beta_{e0} = 8\pi p_{e0}/B^2$ , independent of  $\hat{A}$  (Fig. 4c).

The predictions of the model can be compared with several key observations in the magnetotail. The isotropic spectrum observed above an energy threshold in the Wind satellite observations<sup>4</sup> results from scattering as particles pass close to X-lines. Particle energies well in excess of the potential drop across the tail<sup>1,2</sup> with dawn–

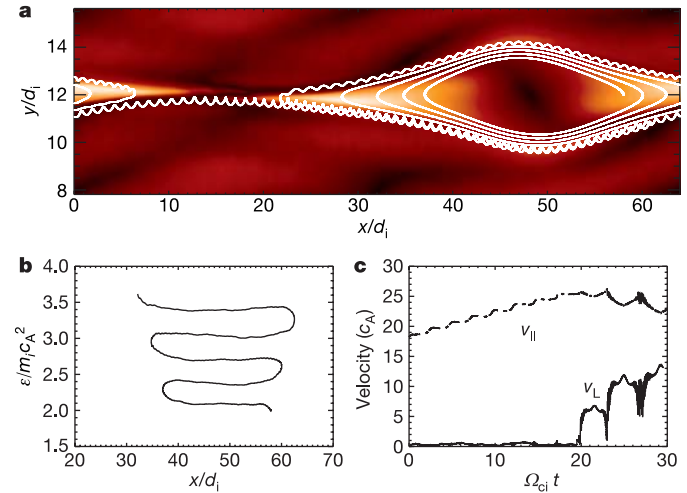


**Figure 2 | Test particle orbits and energy gain of Fermi accelerated electrons.**

The orbits are computed from the fields of the simulation in Fig. 1 at a time  $t = 10.8\Omega_{ci}^{-1}$ , just before the formation of secondary islands. **a**, The orbit of a particle started at the midplane on the right side of the upper island  $x, y = 58.0d_i, 12.0d_i$  with an initial velocity given by the local  $\mathbf{E} \times \mathbf{B}$  velocity plus a parallel velocity  $v_{\parallel}$  of  $10.8c_A$  shown on the background of  $E$ . The particle follows field lines and slowly drifts outward. **b**, The particle energy  $\varepsilon$  as a function of its  $x$  position. The particle gains energy as it reflects from the ends of the islands, which are moving inwards at the Alfvén speed. The energy gain therefore results from a classical Fermi reflection. Because the velocity of energetic electrons greatly exceeds the Alfvén speed, many reflections are required for electrons to reach high energy. Also evident in **a** is the sudden change in the orbit as the island approaches the separatrix—the gyration radius of the particle abruptly increases as the particle encounters the sharp kink in the magnetic field line just downstream from the X-line at  $x, y = 16d_i, 12d_i$ . **c**, The parallel velocity,  $v_{\parallel}$ , which increases in time until  $t = 20\Omega_{ci}^{-1}$  when the local gyration velocity  $v_{\perp}$  abruptly increases. The separatrix crossing therefore scatters energy from the parallel into the perpendicular motion<sup>10</sup>. The energy gain during the reflection from the island ends in **b** can be calculated in a simple model in which  $B_y$  and  $B_z$  are constant and  $B_x(y)$  increases away from the centre of the current layer. The reconnection field  $E_z$  and an in-plane electric field  $E_y = -E_z B_z/B_y$  are chosen so that  $\mathbf{E}_{\parallel} = \mathbf{b} \cdot \mathbf{E} = 0$ . For electrons with  $v_{\parallel} \gg v_{\perp}$ , the change in the parallel velocity results from the curvature drift in the direction of the electric field,  $dv_{\parallel}/dt = cv_{\parallel} \mathbf{E} \cdot \mathbf{b} \times \kappa/B$  where  $\kappa = \mathbf{b} \cdot \nabla \mathbf{b}$ . This equation can be integrated to obtain the increment in the parallel velocity  $\delta v_{\parallel} = -2u_x B_x/B$  due to its reflection, where  $u_x = -cE_z/B_y$  is the local velocity of the end of the island and  $B_x$  is given by its asymptotic value. The resulting rate of energy gain is given in equation (1).

dusk asymmetries that are weak during storm times<sup>3,18</sup> require an acceleration mechanism that can diffuse particles downward and duskward while still gaining energy. In the Fermi model, the particle energy gain is independent of the sign of  $v_{\parallel}$  and therefore independent of the direction of motion across the tail. Thus, there is no intrinsic limit on the energy gain. Distributions of high-energy particles in the magnetosphere are typically power laws, consistent with Fig. 4c. Remarkably, the model yields a spectral index for energetic particles of 3.7 for the Wind parameters, which is close to the measured value of 3.8 (ref. 4).

An important conclusion from solar satellite observations is that up to half of the energy released during solar flares is transferred to electrons. In the data presented in Fig. 4, the electrons receive the bulk of the released magnetic energy in the core of the multi-island region. In the low  $\beta_{e0}$  regime of the corona, the spectral index of energetic electrons approaches a lower limit of 1.5, a spectrum that is hard but is occasionally observed<sup>19</sup>. As essentially all of the electrons entering the multi-island region through the area  $S = \Delta_x \times \Delta_z$  in Fig. 4a undergo significant acceleration, rates of energetic electron production of  $10^{36} \text{ s}^{-1}$  as inferred from observations<sup>20</sup> are possible but only if  $S$  is macroscopic ( $n = 10^9 \text{ cm}^{-3}$ ,  $u_y = 0.1c_{Ax}$ ,  $B = 100 \text{ G}$  and  $S = 10^{19} \text{ cm}^2$ , yields  $\dot{N} = nu_y S \sim 10^{36} \text{ s}^{-1}$ ). Some solar observations do reveal island-like structures in macroscale current layers<sup>21</sup>.

Data from the present fleet of magnetospheric satellites should be able to validate key features of the present model. Secondary

magnetic islands in the vicinity of the dissipation region are required for the production of very energetic electrons and should be measurable in the existing data sets. Secondary islands and energetic electrons should not be produced unless the ambient electron pressure is small ( $\beta_{e0} = 8\pi p_{e0}/B^2 \ll 1$ ).

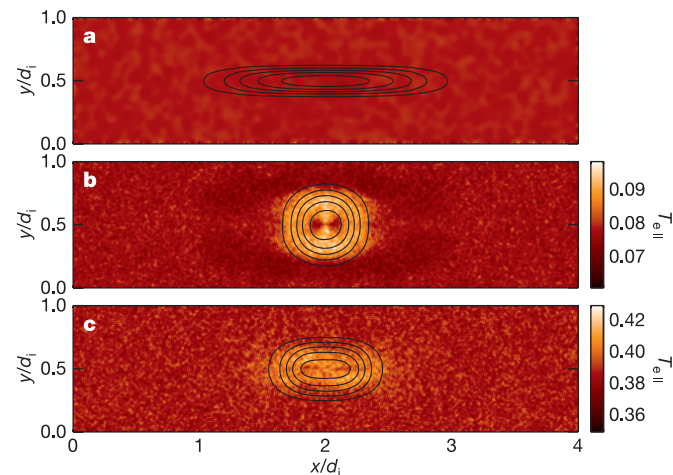


**Figure 3 | Electron Fermi acceleration in squashed flux bubbles.** Shown are the results of two-dimensional simulations of electron acceleration in isolated, squashed flux bubbles, where Fermi acceleration can be studied without the interference from the parallel electric fields associated with magnetic reconnection. The release of magnetic energy as the bubbles contract and become round is essentially the same as in the contraction of magnetic islands during magnetic reconnection. **a**, The initial magnetic field lines in a squashed magnetic bubble superimposed over the uniform, isotropic electron temperature  $T_{e0} = 0.1$ . The bubble is initially in force balance in the  $y$  direction (the variation in the density enabling the plasma pressure to balance the magnetic pressure) but not in the  $x$  direction. Initially  $\beta_{e0} = 8\pi n_0 T_{e0}/B_0^2 = 0.27$ , where  $n_0$  and  $B_0$  are the maximum values of the density and magnetic field, and  $B_z$  is zero. Realistic values of the electron mass ( $m_i/1,836$ ) and velocity of light ( $c = 100c_A$ ) are required so the electrons can undergo many Fermi reflections during the contraction of the bubble. **b**, The parallel electron temperature  $T_{e\parallel}$  and magnetic field lines at late time. Note the increase in the parallel temperature within the bubble and the near circular shape of the final magnetic field lines. The change in the perpendicular temperature is small. Sixty percent of the released magnetic energy is transferred to electrons. **c**,  $T_{e\parallel}$  and the magnetic field lines at late time shown from a simulation that is identical to that shown in **a** and **b** but with a larger initial electron pressure ( $\beta_{e0} = 1.1$ ). In this case, the back pressure from the accelerated electrons prevents the full contraction of the bubble, consistent with the discussion following equation (2).

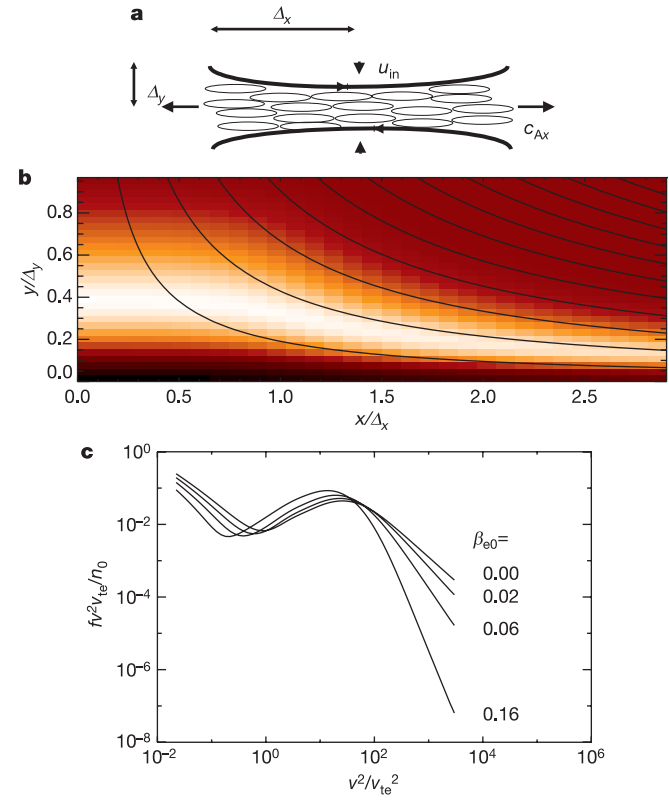


**Figure 4 | Particle acceleration in a multi-island reconnection geometry.** **a**, Diagram showing volume filling islands expected around the reversal region, where owing to incompressibility the inflow velocity is given by  $u_{in} = c_{Ax}\Delta_y/\Delta_x$ . To calculate electron acceleration, we average the energy gain in equation (1) over many islands, including the scattering of energy from the parallel to the perpendicular direction:

$$\frac{d\varepsilon}{dt} = \frac{2\varepsilon}{3} \left\langle \frac{B_{xi}^2 c_{Ax}}{B_i^2 \delta_{xi}} \right\rangle = 2 \frac{A\varepsilon}{3} \frac{dc_{Ax}}{dy} \quad A \equiv \left\langle \frac{B_{xi}^2 \delta_{yi}}{B_i^2 \delta_{xi}} \right\rangle$$

where the contraction velocity of each island is the upstream Alfvén speed  $c_{Ax}$  and  $\delta_{yi}$  is the island width. The subscript “ $i$ ” indicates that the value can vary among the different islands. The resulting equation for the omnidirectional distribution function  $F(x,y,v)$  is solved numerically. One quadrant ( $x,y > 0$ ) of  $F(x,y,1.95v_{te})$  is shown in **b** along with the streamlines of the flow for  $\hat{A} = 0.6$  and  $\beta_{e0} = 0.02$ , where  $v_{te}$  is the initial thermal velocity of the upstream Maxwellian distribution. The white band results from the heating of inflowing low energy electrons and the dark band from the depletion of these particles as they move to even higher energies. **c**, Energy spectra for  $\hat{A} = 0.6$  and several values of  $\beta_{e0}$  at  $x,y = 0,0$ . The spectra are power laws at high energy with spectral indices  $\sigma$  of 1.3, 1.7, 2.2 and 3.7 for  $\beta_{e0} = 0.0, 0.02, 0.06$  and  $0.16$ , respectively. The dip results from the depletion of particles undergoing acceleration to higher energy. For  $\hat{A} = 0.6$ , the energy integrals of the spectra diverge in the absence of the back pressure from energetic particles (the  $\beta_{e0} = 0.0$  spectrum in **c** matches the  $\sigma = 1.33$  prediction from equation (4)). For any finite  $\beta_{e0}$  the back pressure from the energetic particles reduces the drive to regularize the energy spectrum. The limiting spectral index for low  $\beta_{e0}$  is 1.5. Higher values of  $\beta_{e0}$  yield softer spectra with  $\sigma = 3.7$  for the case  $\beta_{e0} = 0.16$ , close to the measured value of 3.8 at  $\beta_{e0} = 0.16$  from the Wind energetic particle observations<sup>4</sup>. In the strongly driven regime ( $\hat{A} > 0.5$ ), the power-law indices are nearly independent of  $\hat{A}$ . The ambient value of  $\beta_{e0}$  is therefore the dominant control parameter for the spectra of energetic electrons during magnetic reconnection.

Received 30 August 2005; accepted 19 July 2006.

1. Terasawa, T. & Nishida, A. Simultaneous observations of relativistic electron bursts and neutral-line signatures in the magnetotail. *Planet. Space Sci.* **24**, 855–856 (1976).
2. Baker, D. N. & Stone, E. C. Energetic electron anisotropies in the magnetotail: identification of open and closed field lines. *Geophys. Res. Lett.* **3**, 557–560 (1976).
3. Meng, C.-I., Lui, A. T. Y., Krimigis, S. M. & Ismail, S. Spatial distribution of energetic particles in the distant magnetotail. *J. Geophys. Res.* **86**, 5682–5700 (1981).
4. Øieroset, M., Lin, R. P., Phan, T. D., Larson, D. E. & Bale, S. D. Evidence for electron acceleration up to 300 keV in the magnetic reconnection diffusion region in the earth's magnetotail. *Phys. Rev. Lett.* **89**, 195001 (2002).
5. Lin, R. P. & Hudson, H. S. 10–100 keV electron acceleration and emission from solar flares. *Sol. Phys.* **17**, 412–435 (1971).
6. Lin, R. P. *et al.* RHESSI observations of particle acceleration and energy release in an intense solar gamma-ray line flare. *Astrophys. J.* **595**, L69–L76 (2003).
7. Drake, J. F., Swisdak, M., Schoeffler, K. M., Rogers, B. N. & Kobayashi, S. Formation of secondary islands during magnetic reconnection. *Geophys. Res. Lett.* **33**, L13105, doi:10.1029/2006GL025957 (2006).
8. Pritchett, P. L. & Coroniti, F. V. Three-dimensional collisionless magnetic reconnection in the presence of a guide field. *J. Geophys. Res.* **109**, A01220, doi:10.1029/2003JA009999 (2004).
9. Drake, J. F., Shay, M. A., Thongthai, W. & Swisdak, M. Production of energetic electrons during magnetic reconnection. *Phys. Rev. Lett.* **94**, 095001 (2005).
10. Buechner, J. & Zelenyi, L. M. Regular and chaotic particle motion in sheared magnetic field reversals. *Adv. Space Res.* **11**, 177–182 (1991).
11. Birn, J., Thomsen, M. F. & Hesse, M. Electron acceleration in the dynamic magnetotail: Test particle orbits in three-dimensional magnetohydrodynamic simulation fields. *Phys. Plasmas* **11**, 1825–1833 (2004).
12. Matthaeus, W. H., Ambrosiano, J. J. & Goldstein, M. J. Particle acceleration by turbulent magnetohydrodynamic reconnection. *Phys. Rev. Lett.* **53**, 1449–1452 (1984).
13. Kliem, B. Particle orbits, trapping and acceleration in a filamentary current sheet model. *Astrophys. J.* **90**, 719–727 (1994).
14. Galeev, A. A., Kuznetsova, M. M. & Zelenyi, L. M. Magnetopause stability threshold for patchy reconnection. *Space Sci. Rev.* **44**, 1–41 (1986).
15. Shibata, K. & Tanuma, S. Plasmoid-induced-reconnection and fractal reconnection. *Earth Planets Space* **53**, 473–482 (2001).
16. Jokipii, J. R. & Parker, E. N. Stochastic aspects of magnetic field lines of force with application to cosmic-ray propagation. *Astrophys. J.* **155**, 777–798 (1969).
17. Blandford, R. D. & Eichler, D. Particle acceleration at astrophysical shocks: a theory of cosmic ray origin. *Phys. Rep.* **154**, 1–75 (1987).
18. Imada, S., Hoshino, M. & Mukai, T. in *Frontiers in Magnetospheric Plasma Physics: Celebrating 10 Years of Geotail Operation* (eds Hoshino, M., Omura, Y. & Lanzerotti, L. J.) 34–39 (Cospar Colloquia Series Vol.16, Elsevier, Oxford, 2005).
19. Holman, G. D. Energetic electrons in solar flares as viewed in x-rays. *Adv. Space Res.* **35**, 1669–1674 (2005).
20. Miller, J. A. *et al.* Critical issues for understanding particle acceleration in impulsive solar flares. *J. Geophys. Res.* **102**, 14631–14659 (1997).
21. Lin, J. *et al.* Direct observations of the magnetic reconnection site of an eruption on 2003 November 18. *Astrophys. J.* **622**, 1251–1264 (2005).
22. Zeiler, A. *et al.* Three-dimensional particle simulations of collisionless magnetic reconnection. *J. Geophys. Res.* **107**, 1230, doi:10.1029/2001JA000287 (2002).

**Supplementary Information** is linked to the online version of the paper at [www.nature.com/nature](http://www.nature.com/nature).

**Acknowledgements** This work was supported by the NSF/DOE programme in plasma science, by NASA through the Supporting Research and Technology and the Sun-Earth Connections Theory programmes, through CMPD, a DOE FSC, and through CISM, an NSF STC. Computations were carried out in part at the National Energy Research Scientific Computing Center.

**Author Contributions** J.F.D., M.S. and M.A.S. identified the Fermi mechanism; J.F.D. carried out the particle simulations of reconnection, obtained the solutions of the transport equation and wrote the paper; and M.S. and H.C. carried out the bubble and test particle simulations, respectively. All of the authors discussed the results and commented on the paper.

**Author Information** Reprints and permissions information is available at [www.nature.com/reprints](http://www.nature.com/reprints). The authors declare no competing financial interests. Correspondence and requests for materials should be addressed to J.F.D. (drake@plasma.umd.edu).